RECEIVED BY TIC JUL - 2 1979

SAND 79-0074
Unlimited Release

MASTER

THERMAL EXPANSION AND DENSITY MEASUREMENTS OF MOLTEN AND SOLID MATERIALS AT HIGH TEMPERATURES BY THE GAMMA ATTENUATION TECHNIQUE

William D. Drotning

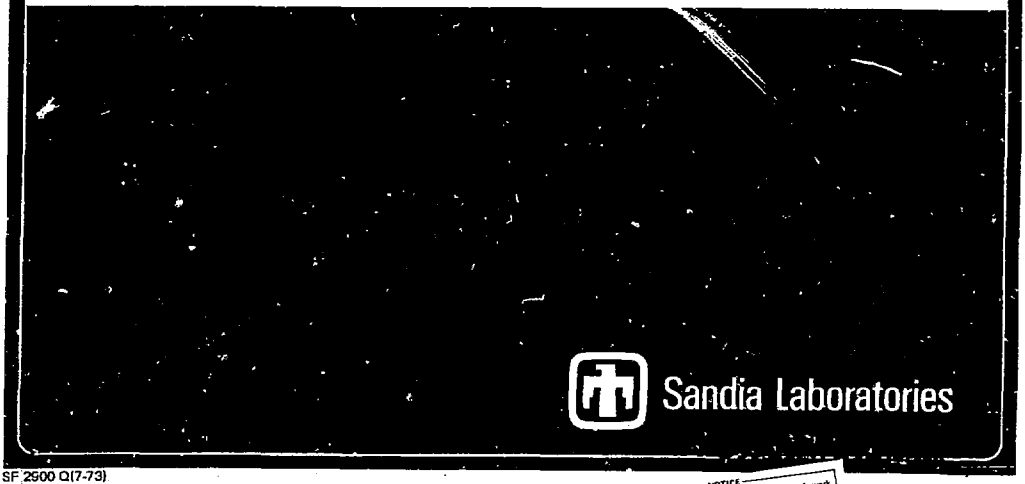

SF 2900 Q(7-73)

NOTICE
This report was prepared as an account of work sponsored by the United States Government. Neither the United States nor the United States Department of Energy, nor any of their employees, nor any of their contractors, subcontractors, or their employees, makes any warranty, express or implied, or assumes any legal liability or responsibility for the accuracy, completeness or usefulness of any information, apparatus, product or process disclosed, or represents that its use would not infringe privately owned rights.

THERMAL EXPANSION AND DENSITY MEASUREMENTS OF MOLTEN AND SOLID MATERIALS AT HIGH TEMPERATURES BY THE GAMMA ATTENUATION TECHNIQUE

William D. Drotning
Thermophysical Properties
Division 5842

Abstract

An apparatus is described for the measurement of the density and thermal expansion of molten materials to 3200 K using the gamma attenuation technique. The precision of the experimental technique was analytically examined for both absolute and relative density determinations. Three analytical expressions used to reduce data for liquid density determinations were evaluated for their precision. Each allows use of a different set of input data parameters, which can be chosen based on experimental considerations. Using experimentally reasonable values for the precision of the parameters yields a similar resultant density precision from the three methods, on the order of 0.2%. The analytical method for measurements of the linear thermal expansion of solids by the gamma method is also described. To demonstrate the use of the technique on reasonably well-characterized systems, data are presented for 1) the density and thermal expansion of molten tin, lead and aluminum to 1300 K, 2) the thermal expansion of solid aluminum to the melting point, and 3) the thermal expansion of a low melting point glass through the transition temperature and melting region. The data agree very well with published results using other methods where such published data exist.

Table of Contents

I. INTRODUCTION

The density and thermal expansion of high temperature molten materials are useful for a variety of scientific and technological interests. Besides their inherent value, these properties are also used in calculations of other properties, such as viscosity, surface tension, thermal conductivity, and a variety of heat transfer dimensionless numbers. An example of the technological need for these data is in post-accident heat transfer analysis of molten structural, coolant, and fuel materials for use in nuclear reactor safety studies.

The gamma radiation attenuation technique for density determinations of molten materials offers several advantages over other methods at high temperatures. First, the gamma beam offers a probe which is not in thermal or physical contact with the liquid. This makes the technique particularly advantageous for very high temperature measurements, since thermal losses are minimized, and a probe-sample compatibility problem does not exist. In addition, since a free liquid surface is not involved in the measurement, a number of problems of other methods are eliminated, including sample volatilization, formation of oxide surface films, and corrections for surface tension, liquid/solid interactions, and viscosity effects.

Though the technique itself is not new, it has not achieved widespread use for measurement of thermal expansion or density at high temperatures. Dillon, et al. [1] and LeVert, et al. [2] have reported its use for density measurements of liquid alkali metals, and Döge [3] has used the technique for density measurements in the Pb-Sn system to 1400 K. The densities of liquid lead, cesium, and gallium were examined with the gamma method to 1400 K by Basin and Solov'ev [4]. More recently, the technique has been extended to

studies of iron and copper to 1900 K by Yavoyskiy, et al. [5]. The technique has also been used extensively for determining the bulk density and water content of soils [6,7], and for other technological uses at ambient temperature [8].

In this paper, an experimental apparatus using the gamma attenuation method to 1300 K is described, including the details of the electronic counting system. The extension of the technique to the 3200 K temperature range using a high temperature furnace facility is also described. Sample size and gamma source choice considerations are also presented. Next, the basic equation of the method is presented in forms useful for data analysis, including both relative and absolute density determinations. An analysis of the precision of the method is also given. It is shown that the technique may also be applied to the measurement of the linear thermal expansion of solid materials at high temperature. The technique is unique in that it allows measurements on both solid and liquid phases without a change in measurement technique.

To illustrate the versatility of the measurement technique, data are presented for the volumetric thermal expansion from the melting point to 1300 K of molten tin, lead, and aluminum, and the linear thermal expansion of solid aluminum. Data are also shown for the density of a low melting point glass versus temperature.

II. EXPERIMENTAL APPARATUS

A. Basic Experimental Method

With this technique, the density of a material is determined from the attenuation which is produced by the passage of a collimated beam of mono-energetic gamma radiation through the material, whose length and absorption coefficient have been independently determined. A schematic of the experimental arrangement for measurements to 1300 K is shown in Fig. 1. A ^{137}Cs 0.662 MeV gamma source (activity 4 Ci) is housed in a lead vault, which provides both radiological shielding and the initial collimation for the gamma beam. A collimator of stainless steel, inside diameter 6.4 mm, directs the beam into the high temperature tubular furnace. The molten material is contained in a crucible supported by a ceramic pedestal, both of which are contained in a controlled-atmosphere (vacuum or inert gas) ceramic chamber. The alignment of the crucible and pedestal is achieved using a He-Ne laser beam passing through the collimators, prior to lowering of the furnace over the chamber. Emerging from the furnace, the beam is further collimated (aperture 6.4 mm) before striking the NaI(Tℓ) scintillation detector, which is shielded in lead. Steel filters of various thicknesses are inserted into the beam to establish an appropriate gamma flux for the detection system.

The basic equation which describes the gamma beam intensity and thus defines the analytical method is [9]

$$I = I_o \exp [-u\rho\ell] \quad , \tag{1}$$

for mono-energetic gammas and a narrow beam (well-collimated) geometry. In Eq. (1), I_o and I are the gamma intensities before and after passage through the sample material, ρ is the material density, ℓ the material length along the beam direction, and u the mass attenuation coefficient of the material.

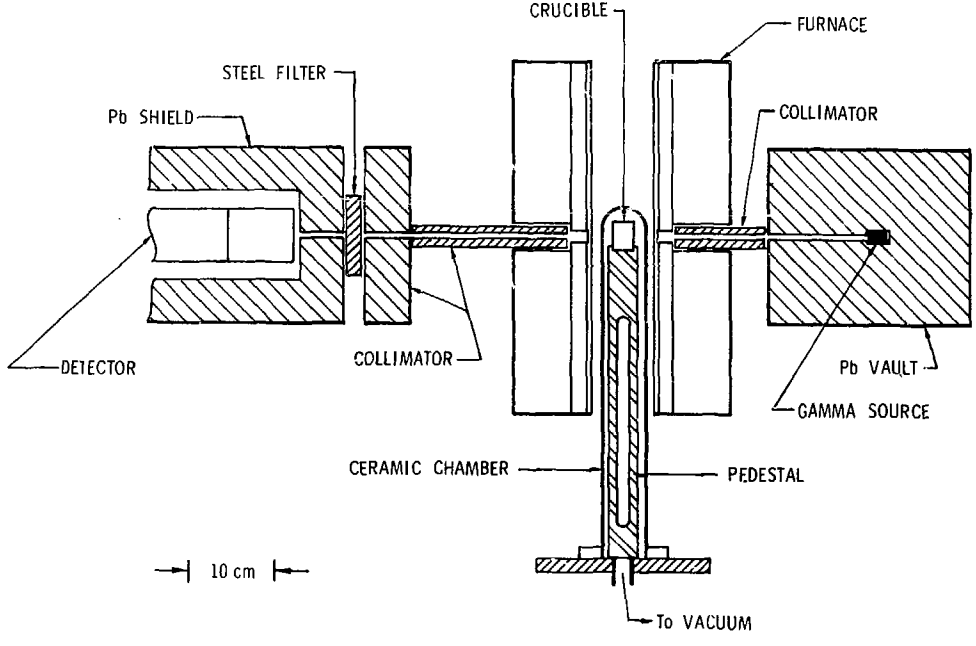

Figure 1. Schematic diagram of gamma attenuation experimental apparatus. The furnace shown here has a range from ambient to 1300 K.

B. Gamma Detection Apparatus

The gamma detection system is outlined in Fig. 2; except for the scintillation detector (Bicron 3M3P), the apparatus was manufactured by Canberra Industries, Inc., Meridan, Conn. The detector consists of a NaI (Tℓ) crystal (76.2 mm diam. x 76.2 mm length), hermetically attached to a photomultiplier tube window. To achieve count rate stability over extended time periods, the temperature of the detector is thermostatically-controlled to within ±0.1°C using a circulating air bath heated slightly above ambient temperature. The output pulses are amplified and shaped by the preamplifier (Model 802-9) and amplifier (Model 2010). The amplified pulses pass through a digital stabilizer (Model 1720), which offers automatic gain control of the linear electronics. This device was found necessary to provide system counting stability over long time periods (several hours). The stabilizer compensates for gain shifts in the system due to line voltage variations, high voltage power supply (HVPS) variations, count rate changes, and ambient temperature variations. The single channel analyzer (Model 2030) passes the pulses in the ^{137}Cs photopeak to the counter (Model 1790C). The output is also interfaced to a computer-based data acquisition system for real-time monitoring of sample temperature and count rate, as well as subsequent data analysis.

The precision to which the beam intensity is measured is limited by the statistics which govern the random nuclear emission process. The measurement uncertainty decreases as $1/\sqrt{N}$ for a total number of accumulated counts N. A count rate limit of about 40,000 counts per second (cps) is imposed to accommodate the detection electronics. At this rate, data accumulation for ten minutes yields a count rate precision of about 0.02%. Using both the automatic gain stabilizer and the thermostated detector, a stabilized detection system

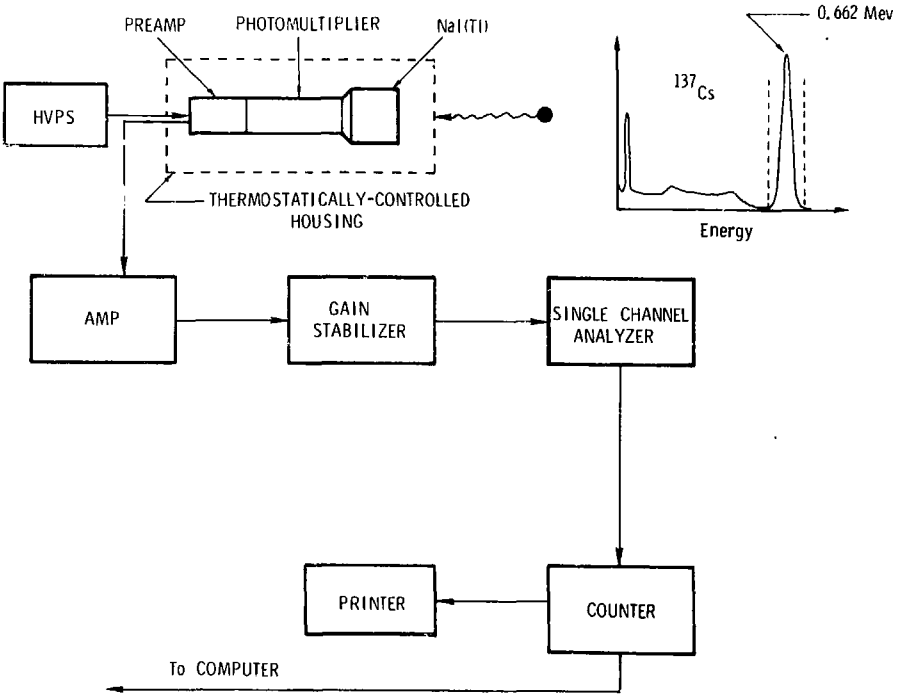

Figure 2. Block diagram of gamma detection apparatus.

has been achieved. For count rates above 1000 cps, a correction is required for the "dead time" of the electronics system; this originates from the probability of a second pulse occurring while the detection system analyzes a first pulse [9].

C. Furnace Facilities

The low temperature apparatus utilizes a resistance-type tubular furnace, as shown in Fig. 1, to achieve sample temperatures from ambient to 1300 K. The furnace was modified by drilling collimator clearance holes into the furnace jacket and insulation. The furnace resistance wires were also drilled out and subsequently bypassed in the beam region. Thermocouple thermometry (Type K) is used to monitor and control the sample temperature.

For temperatures to 3200 K, a high temperature controlled-atmosphere tungsten mesh furnace (Astro Model 1100V, Astro Industries, Inc., Santa Barbara, CA) is used instead of the tubular furnace. A horizontal cross-section of the furnace is shown in Fig. 3. The collimated gamma beam is aligned to pass through sight port holes in the radiation shield pack and through the electrode gaps in the tungsten mesh heater element. Sample temperature is determined by optical pyrometry, viewed through a sight port in either the side or the top of the furnace; the necessary correction is made for the transmission of the viewing optics.

D. Samples

In principle, the samples may be either liquid or solid, with cylindrical or rectangular shape. Molten density measurements using the gamma technique require either the ambient temperature sample density and dimension with which to compute u, or an independent measure of the sample density at one temperature when molten (e.g., at the melting point).

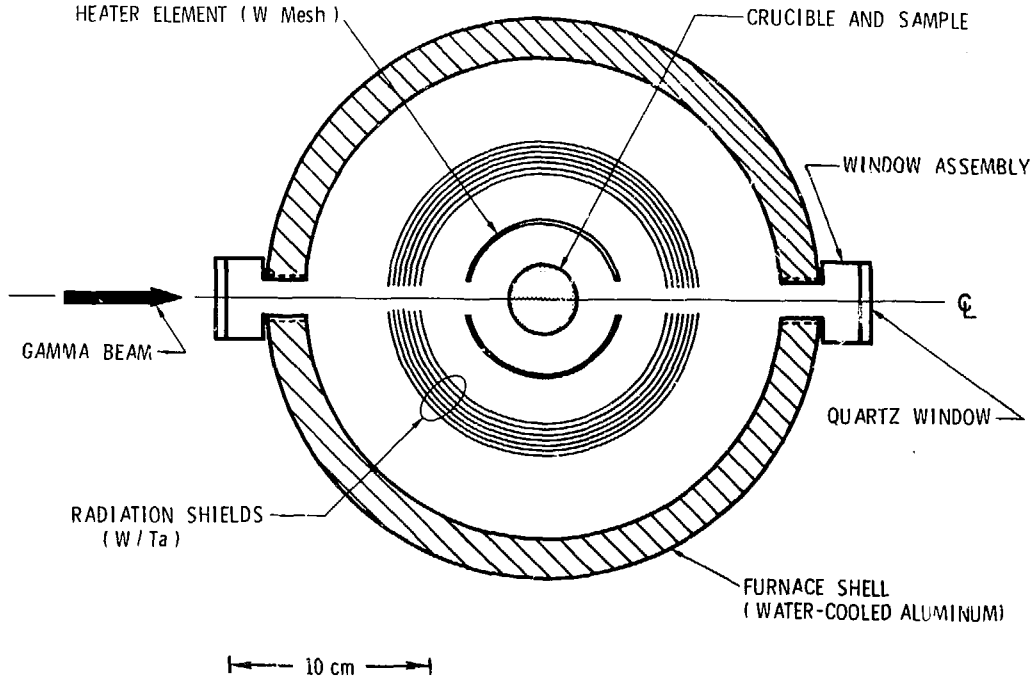

Figure 3. Horizontal cross-section of the Astro high temperature furnace, for temperatures to 3200 K. The drawing is approximately one-half scale. The gamma beam is aligned to pass through port holes in the radiation shields and the electrode gap in the heater element.

Sample-crucible compatibility should be considered; if the crucible is attacked, the composition of the sample may change along with the crucible dimension. Compositional uniformity in complex materials may also be of concern. Depending on the sample and atmosphere, vapor deposition onto internal chamber walls may be a source of a temperature (and time) dependent I_o or may cause a reduction in furnace efficiency and a loss of sample material. This can be reduced significantly by using crucible lids or sealed containers.

While a large sample size eases alignment and improves measurement sensitivity, small samples equilibrate faster, with smaller temperature gradients. In the molten phase, natural convection will speed thermal equilibration. Accurate knowledge of the sample temperature is necessary for reporting density results, while precise measurement of temperature differences is important for determination of thermal expansion coefficients.

For the low temperature apparatus, sample sizes are nominally cubical, 2 cm on a side. In the Astro furnace, larger samples may be accommodated, up to cylinders nominally 3 cm diameter by 5 cm long.

E. Crucibles

For the 1300 K apparatus, crucibles are precision-machined from high-purity graphite or boron nitride into rectangular shapes with sides parallel to each other and perpendicular to the beam direction. Flat-wall crucibles are easier to align and contribute little uncertainty to the sample length along the beam axis. A variety of other crucible materials are available for use in the high temperature Astro furnace, including magnesia, alumina, zirconia, thoria, beryllia, molybdenum, tantalum, and tungsten. The choice of crucible

material is determined by sample-crucible compatibility, maximum use temperature, high temperature strength, thermal shock resistance, crucible vapor pressure, cost and availability, to name a few.

The refractory ceramic and metal crucibles are typically cylindrically-shaped, so that crucible alignment becomes more critical. An analysis was made (see Appendix A) to calculate an effective pathlength through a cylindrical crucible, including the error due to off-center alignment. Depending on the data analysis method, the inside dimension of the crucible along the beam direction may need to be known precisely at some temperature. The porosity and roughness of the crucible walls also affect the precision of this dimension measurement. For containment of corrosive liquids at high temperatures for long periods, the possibility of a changing crucible dimension, due to surface attack, should also be considered. In most cases, thermal expansion data for the crucible material is available to sufficient accuracy to allow the necessary pathlength correction.

F. Optimization of Sample Length and Gamma Source

Equation (1) may be used to determine an optimum sample length and gamma energy. As the product $(u\rho\ell)$ in Eq. (1) increases, the attenuation increases, and the uncertainty in ρ due to imprecision in I decreases. On the other hand, as $(u\rho\ell)$ increases, the count rate diminishes, so that longer times are required to yield a given precision; thus, there exists an optimum $(u\rho\ell)$. Considering only uncertainties due to measurement of I and I_o, one can show that, for a fixed total counting time, the fractional standard deviation for ρ is a minimum at $(u\rho\ell) = 2$. (This value also minimizes the counting time necessary to achieve a given precision [7].)

The criterion ($u\rho\ell$) = 2 can be used for selection of a sample length ℓ and the gamma source, since u varies with gamma energy as well as with atomic number Z. For ℓ = 3 cm and densities which range from 5 to 15 g/cm^3, the above criterion gives u ~0.13 to 0.04 cm^2/g. A source is desired which has 1) a long isotope half-life, 2) a relatively simple energy spectrum, giving a strong, monochromatic beam with no higher energy peaks contributing Compton scattered photons, and 3) a high specific activity. As a practical matter, source cost, availability, and shielding requirements eliminate many choices. With these considerations, ^{137}Cs emerges as the best source for most applications. At the ^{137}Cs energy of 0.662 MeV, u is ~ 0.07 cm^2/g, and relatively independent of material Z.

C. Refinements to The Basic Equation

To apply Eq. (1) to the determination of density from experimental data, some refinements are necessary which have not been universally recognized in some of the previous density/thermal expansion literature. These will now be discussed.

1. Dead time. The refinement of Eq. (1) to include the dead time of the counting system has been ignored in some earlier works. The actual (corrected) count rate I (or I_o) differs from the measured (uncorrected) count rate R (or R_o) by the equation [9]

$$I = \frac{R}{1 - R\tau} \quad , \tag{2}$$

where τ is the dead time of the counting system. For a given apparatus (fixed τ), the difference between I and R depends on the rate R and will become negligible for small R.

An experimental determination of the counting system dead time τ is necessary, since τ depends on the instruments and their particular settings. The two-source method [10] was used to determine τ. Count rates were measured for irradiation by each of two sources separately, R_1 and R_2, and for both sources simultaneously, R_{12}. Using Eq. (2) and the condition $I_1 + I_2 \approx I_{12}$ yields,

$$\tau = R_{12}^{-1}\left\{1 - \left[1 - \frac{R_{12}}{R_1 R_2}(R_1 + R_2 - R_{12})\right]^{\frac{1}{2}}\right\} \quad . \tag{3}$$

The apparatus described here has $\tau \sim 3$ μsec; thus, for R ~ 40,000 cps, I is approximately 12% larger than R.

2. Temperature-dependent I_o. One should recognize that I_o, the (corrected) count rate in the absence of the sample material, can itself be represented by an equation of the form Eq. (1), where $(u\rho\ell)$ is replaced by $\sum_i u_i\rho_i\ell_i$, and the subscripts denote the materials in the path of the gamma beam (furnace walls, vacuum chamber walls, crucible walls, etc.). It is then clear that I_o will be a function of temperature, since $\rho_i\ell_i$ will vary as the temperature of each material changes. In addition, temperature can be expected to vary the size of collimation apertures as well, causing an additional dependence of I_o on T. These effects are taken into account by measurement of $R_o(T)$ as a function of temperature.

For the 1300 K apparatus shown in Fig. 1, the temperature dependence of I_o was experimentally determined; a complete modeling of the attenuation due to the various materials in the beam is quite complex, since exact temperatures of each material at various equilibrium temperatures are required. In addition, the expansion of the collimators must also be included, and these have large temperature gradients along them. The count rate I_o was empirically found to increase linearly with temperature as

$$I_o(T) = I_o(T_1) \times \left[1 + \varepsilon(T - T_1)\right] \quad , \tag{4}$$

where T_1 is ambient temperature. Using graphite crucibles of total wall thickness nominally 3.5 mm yields $\varepsilon \approx 4 \times 10^{-6}$/K. About 15% of this change in I_o is due to the expansion of the crucible itself (see Appendix B).

With the high temperature Astro furnace, the temperature dependence of I_o was measured and found to be entirely due to the expansion of the crucible. Fig. 3 shows that this should be the case, since the only other material (besides inert gas) in the beam's path is the quartz in the windows. Since these are water cooled, their attenuation does not change with sample temperature. For this furnace, then, a calculation based on crucible wall thickness and expansion is sufficient to predict the temperature dependence of I_o (see Appendix B).

3. Crucible Expansion. Besides affecting $I_o(T)$, thermal expansion of the crucible also changes the sample dimension along the beam axis, when the sample is in the liquid phase. This is easily taken into account using available data on mean expansion coefficients for crucible materials.

Taken altogether, these refinements lead to a modified form of Eq. (1) given by,

$$I(T) = I_o(T) \quad \exp\left\{-u\rho(T)\ell_1\left[1 + \alpha(T - T_1)\right]\right\} \quad , \tag{5}$$

where $I(T)$ and $I_o(T)$ are determined from measured (uncorrected) count rates using Eq. (2). The sample temperature is T, ℓ_1 is the sample length at T_1, and α is the mean linear expansion coefficient of the crucible over the range T_1 to T. Eq. (4) may be used to find $I_o(T)$.

H. Mass Attenuation Coefficient

The mass attenuation coefficient is independent of the physical state of the material and therefore is independent of temperature. However, since u results from both atomic absorption and scattering pro ..s, its value may be slightly dependent on the measurement geometry. Becaus. accurate values of u may be lacking for a given material, it is advisable to measure u experimentally for each material investigated. This can usually be done at room temperature by measuring I through a length L of the material; then u is calculated from

$$u = \frac{1}{\rho L} \ln(I_o/I) \quad . \tag{6}$$

The uncertainty in u results from the uncertainty in ρ and L for the material, since, in principle, one can count indefinitely at room temperature and thereby determine I_o and I to any precision. Mass attenuation coefficients may also be calculated [11] for elements, mixtures, and compounds from literature data. These values are typically within 2% of the experimental values.

I. Additional Experimental Considerations

An identification and discussion of several experimental conditions which contribute to both systematic and random errors in the gamma attenuation method are presented in this section. The gamma source decays with time, leading to a time-varying count rate. For ^{137}Cs, with a half-life of 30 years, the correction is ~2.5 cps (.006%) change per day for a rate of 40,000 cps. In most instances, this can be ignored. The length of beam collimators should be considered, since the analysis requires a narrow-beam geometry. If the collimators are too short, beam divergence at the sample can systematically influence the results, since gammas scattered through large angles will be

detected (the so-called "build-up factor" [9]). The effective sample length will then be larger than its physical length. For this reason, it is desirable to measure u_{ℓ} for each sample with the same collimation used throughout, thus insuring an unchanging beam geometry. For a well-collimated beam, and $(u\rho\ell) \sim 1\text{-}2$ (so that the gamma mean free path in the sample is ~1), the build-up factor in the sample may be neglected.

For a source (unlike ^{137}Cs) with gammas of energies above those observed by the electronics, Compton events in the detector can also bias the measured results. Counts caused by background radiation must also be considered; proper shielding can minimize this effect.

In spite of efforts to achieve precision in alignment and positioning of the furnace, collimators, and vacuum chamber, it has been found difficult to repetitively reproduce the gamma flux through the bare apparatus (I_o) to better than 0.1%. This problem results from movement of the furnace and collimators during sample loading with the 1300 K furnace facility. Neither collimators nor furnace are moved during loading of the 3200 K furnace. When accurate I_o data cannot be reproduced, a modified data analysis can be employed, as discussed below.

Drift of the electronics system with voltage and ambient temperature fluctuations can seriously affect count rate reproducibility. The system described above employs a thermostated detector housing and an automatic gain control to eliminate such fluctuations. The count rate stability has been demonstrated to be within ±0.05% for long periods of time (days). This figure represents the oscillation of the count rate (about some mean value), which occurs on a diurnal basis. Better stability might be obtained through temperature control of the electronic counting system, if necessary. The gain control also compensates for system gain shift due to count rate dependence, a

typical problem with nuclear counting systems. An alternative solution is to collect the complete gamma spectrum with a pulse height analyzer and to computer-analyze the counts in the desired peak, regardless of its location. This approach could not be used if the detected gamma peak shifts during the measurement, however.

Detector fatigue or hysteresis may affect the system gain, and thus the measured count rates, if high gamma fluxes are incident [12]. With the above apparatus, these effects were minimized by establishing the procedure of waiting ~30 minutes after drastic rate changes are made before resumption of counting.

III. DATA ANALYSIS METHODS

A. Liquid Density and Thermal Expansion

The gamma attenuation technique can be used to give both absolute and relative liquid density measurements. First, a form is presented for an absolute density determination (Method 1). Solving Eq. (5) for $\rho(T)$ yields

$$\rho(T) = \frac{\ell n[I_o(T)/I(T)]}{u\ell_1[1 + \alpha(T - T_1)]} \quad , \tag{7}$$

where it is understood that I and I_o are determined from measured rates R and R_o using Eq. (2). To employ Eq. (7), u is first determined from Eq. (6). The inside length ℓ_1 and expansion α of the crucible are also required. Next, $I_o(T)$ is measured, and finally, I(T) is measured with the molten sample in the crucible to give $\rho(T)$ by Eq. (7). A number of independent measurements are thus required for this method of analysis.

Another approach (Method 2), which may offer some advantages, is found by solving Eq. (7) for $(u\ell_1)$ at T_1 and equating this expression to the one for another temperature T_2. This leads to

$$\rho(T_2) = \frac{\rho(T_1)}{[1 + \alpha(T_2 - T_1)]} \times \frac{\ell n[I(T_2)/I_o(T_2)]}{\ell n[I(T_1)/I_o(T_1)]} \quad . \tag{8}$$

In Eq. (8), u and the absolute crucible dimension ℓ_1 do not enter the data analysis; instead, this approach requires independent knowledge of $\rho(T_1)$ in the melt from another method and is therefore a relative density method.

A third analytical approach (Method 3, a relative density method) is found by writing Eq. (5) at a temperature T_1 and dividing throughout by Eq. (5) at T_2. One then has

$$\rho(T_2)\ell(T_2) - \rho(T_1)\ell(T_1) = \frac{\ell n[I(T_1)I_o(T_2)/I(T_2)I_o(T_1)]}{u} \quad . \qquad (9)$$

Unlike the previous two equations, this has a term $I_o(T_2)/I_o(T_1)$; if an experimentally-determined expression relating I_o at T_1 and T_2 can be found, some cancellation of terms may result. For I_o weakly-dependent on T, one can expect a functional dependence of the form $I_o(T_2)/I_o(T_1) = f(T_2-T_1)$, such as that shown in Eq. (4), where $f(\Delta T) = 1 + \varepsilon(\Delta T)$. Eq. (9) can then be rewritten as

$$\rho(T_2) = \frac{\rho(T_1)}{1 + \alpha(T_2 - T_1)} + \frac{\ell n[I(T_1)f(T_2 - T_1)/I(T_2)]}{u\ell(T_1)[1 + \alpha(T_2 - T_1)]} \quad . \qquad (10)$$

While this form requires knowledge of $\rho(T_1)$, u, and $\ell(T_1)$, it does not explicitly contain I_o. This may be particularly advantageous if f, the temperature dependence of I_o, is known, but I_o is not. This can readily occur for experimental arrangements where the furnace, controlled atmosphere chamber, and collimators are disturbed during sample loading. In addition, the elimination of I_o in Eq. (10) makes the determination of $\rho(T_2)$ much less sensitive to uncertainties in τ, since $I(T_1)$ and $I(T_2)$ will usually be less disparate than $I(T)$ and $I_o(T)$.

Each of these methods requires knowledge of either ρ at a reference temperature or u. The accuracy to which $\rho(T_2)$ is determined may thus be limited by the error in $\rho(T_1)$ or u. It can be seen, therefore, that the gamma technique may be more useful in determining changes in density rather than the absolute density itself. Either Eq. (7) or (8) above yields a fractional density change

$$\frac{\rho(T_2) - \rho(T_1)}{\rho(T_1)} = \frac{\ell n[I(T_2)/I_o(T_2)]}{[1 + \alpha(T_2 - T_1)]\ell n[I(T_1)/I_o(T_1)]} - 1 \quad . \qquad (11)$$

Of course, this expression is independent of $\ell(T_1)$, u, and an explicit knowledge of $\rho(T)$. Dividing Eq. (11) by $(T_2 - T_1)$ gives the mean volumetric (density) thermal expansion coefficient α_ρ over the range T_1 to T_2. The precision of this value will depend on the count rate precision and a precise knowledge of $(T_2 - T_1)$.

B. Solid Linear Thermal Expansion

To this point, the analysis presented has been restricted to the application of density and thermal expansion measurements of molten materials. However, the technique may also be applied to the measurement of the linear thermal expansion of solid materials. To the author's knowledge, this represents the first use of the gamma technique for such an application. Particularly at very high temperatures, the gamma attenuation technique may prove superior to push-rod dilatometry because of the non-contacting nature of the measurement. In addition, the gamma attenuation technique is unique in that it allows determination of both the linear thermal expansion in the solid state and the volumetric thermal expansion in the liquid state without any sample change or alteration of measurement techniques.

The ability to apply the gamma attenuation technique to the measurement of the linear thermal expansion of solids requires an assumption relating the linear and volumetric expansion coefficients. The measurement technique ultimately determines the product of density and length, $\rho\ell$; an additional relationship is therefore necessary to deduce $\Delta\ell$, the length change along the beam direction. Eq. (1) may be applied to a solid block of sample material, where the intensities I and I_o are dead-time corrected, and no correction is necessary for the expansion of a crucible. Define the quantity z by dividing Eq. (9) by $\rho(T_1)\ell(T_1)$, yielding

$$z = \frac{\ell n[I(T_1)I_o(T_2)/I(T_2)I_o(T_1)]}{\rho(T_1)\ell(T_1)u} = \frac{\rho(T_2)\ell(T_2)}{\rho(T_1)\ell(T_1)} - 1 \quad . \qquad (12)$$

For isotropic materials, the volumetric (density) expansion α_ρ is related to the linear expansion α_ℓ by [13]

$$\alpha_\rho \cong -3\alpha_\ell(1 - 2\alpha_\ell \Delta T) \quad , \tag{13}$$

where α_ρ and α_ℓ are mean values over a temperature interval $\Delta T = T_2 - T_1$, such that

$$\alpha_\ell = \frac{\ell(T_2) - \ell(T_1)}{(T_2 - T_1)\ell(T_1)} \quad . \tag{14}$$

and

$$\alpha_\rho = \frac{\rho(T_2) - \rho(T_1)}{(T_2 - T_1)\rho(T_1)} \quad . \tag{15}$$

The notation is simplified by using $\rho_1 = \rho(T_1)$, etc. Rearranging (14) and (15) gives

$$(\Delta T)\alpha_\ell = \frac{\ell_2}{\ell_1} - 1 \tag{16}$$

and

$$(\Delta T)\alpha_\rho = \frac{\rho_2}{\rho_1} - 1 \quad . \tag{17}$$

Multiplying (16) and (17) gives

$$(\Delta T)^2 \alpha_\ell \alpha_\rho = \left[\frac{\rho_2 \ell_2}{\rho_1 \ell_1} - \frac{\ell_2}{\ell_1} - \frac{\rho_2}{\rho_1} + 1\right] \quad . \tag{18}$$

The right-hand side can be rewritten as

$$(\Delta T)^2 \alpha_\ell \alpha_\rho = \left(\frac{\rho_2 \ell_2}{\rho_1 \ell_1} - 1\right) - \left(\frac{\ell_2}{\ell_1} - 1\right) - \left(\frac{\rho_2}{\rho_1} - 1\right)$$

$$= z - (\Delta T)\alpha_\ell - (\Delta T)\alpha_\rho \qquad (19)$$

Substituting Eq. (13) into (19) gives

$$-3(\Delta T)^2 \alpha_\ell^2 (1 - 2\alpha_\ell \Delta T) = z - (\Delta T)\alpha_\ell + 3(\Delta T)\alpha_\ell (1 - 2\alpha_\ell \Delta T) \qquad (20)$$

which can be rewritten as

$$6x^3 + 3x^2 - 2x - z = 0 \quad , \qquad (21)$$

where $x \equiv (\Delta T)\alpha_\ell$. The procedure, then, involves measuring $I(T_1)$ and independently measuring ρ_1 and ℓ_1 at some T_1, e.g., room temperature. Subsequent measurements of $I(T_2)$ at temperatures T_2 allow determination of z. Finally, x can be found by standard techniques from Eq. (21), yielding the mean linear thermal expansion, α_ℓ, between T_1 and T_2. (Of the three real roots of Eq. (21), only one yields a physically reasonable result.)

IV. PRECISION ANALYSIS

Analytical expressions for the precision of various parameters have been obtained by writing the rms deviation due to the propagation of random errors through the data analysis expressions. If $\sigma(X_i)$ denotes the standard deviation in the parameter X_i, then one has the variance

$$\sigma^2(G) = \sum_i \left(\frac{\partial G}{\partial X_i}\right)^2 \sigma^2(X_i) \qquad (22)$$

for the case where G is a function of the independent parameters X_i.

For typical values of R ~5000 to 40,000 cps, one can readily achieve a count rate precision of 0.02% by counting for 5000 to 625 sec, respectively, where $\sigma(R)/R = 1/\sqrt{N}$ for a total of N counts. Greater precision requires exceedingly long counting times, so that .02% will be used as an experimentally reasonable count rate precision. The various analytical methods described above are now analyzed in terms of their precision.

The precision analysis for τ (using Eq. (3) for G in Eq. (22)) is illustrated with a numerical example. For R_1 = 4000 cps, R_2 = 40,000 cps, R_{12} = 43,100 cps, and a total count time of 18,000 sec (5 hr), τ = 3.00 μsec ± 0.37%. Typically, then, one can achieve τ to better than 0.5%.

The determination of the mass attenuation coefficient u was also analyzed in terms of precision, using Eqs. (6) and (22). As an example, ρ = 7.2 g/cm^3 ± .05%, ℓ = 2 cm ± .05%, R and R_o ± .05%, and τ ± 1% together give u = 0.079 cm^2/g ± .11%. The uncertainty in calculated parameters is usually less sensitive to τ than to other parameters.

The absolute density determination defined by Eq. (7) yields a fractional variance of $\rho(T)$ given by

$$\left(\frac{\sigma(\rho)}{\rho}\right)^2 = [u\rho\ell(T)]^{-2}\left\{\left(\frac{\sigma(R_o)}{R_o}\right)^2 \frac{1}{(1 - R_o\tau)^2} + \left(\frac{\sigma(R)}{R}\right)^2 \frac{1}{(1 - R\tau)^2} + \left(\frac{\sigma(\tau)}{\tau}\right)^2 \left[\frac{R_o\tau}{1 - R_o\tau} - \frac{R\tau}{1 - R\tau}\right]^2\right\} + \left(\frac{\sigma(u)}{u}\right)^2 + \left(\frac{\sigma(\ell_1)}{\ell_1}\right)^2 + (1 + \alpha\Delta T)^{-2}\left[(\Delta T)^2\sigma^2(\alpha) + \alpha^2\sigma^2(T) + \alpha^2\sigma^2(T_1)\right] \quad , \qquad (23)$$

where $\ell(T) = \ell_1(1 + \alpha\Delta T)$, $\Delta T = T - T_1$, and $\ell_1 = \ell(T_1)$.

For comparison of the methods, a standard numerical example is chosen:

$$R = 16000 \text{ cps} \pm 0.02\%$$

$$R_o = 40000 \text{ cps} \pm 0.02\%$$

$$\tau = 3 \text{ μsec} \pm 1\%$$

$$u = 0.07 \text{ cm}^2/\text{g} \pm 0.1\%$$

$$\ell_1 = 2 \text{ cm} \pm 0.05\%$$

$$T_1 = 300 \text{ K} \pm 1\%$$

$$T = 700 \text{ K} \pm 1\%$$

$$\alpha = 7 \times 10^{-6}/\text{K} \pm 10\%$$

These values in Eqs. (7) and (23) yield $\rho(700 \text{ K}) = 7.087 \text{ g/cm}^3 \pm 0.15\%$, where it is noted that u, τ, and ℓ_1 contribute most significantly to $\sigma(\rho)$. The variance contribution from the parameters is summarized in Table I, along with effects of changing some of the parameters. This table, and the following two, give the parameters used in the calculation of $\rho(T)$ by a particular method. Set A defines a particular standard deviation for each parameter,

TABLE I

Method 1. $\rho(T)$ calculated from Eq. (7). Resultant % error in ρ shown for each of four sets of uncertainties in the input data parameters. Sets B, C, and D show the result of changing the % standard deviation from the values in set A. The % standard deviation for a parameter X_i is defined by $100 \times (\sigma(X_i)/X_i)$, where $\sigma(X_i)$ is the standard deviation of the parameter X_i.

Parameter		Set A		% Standard Deviation		
		% Standard Deviation	Variance Contrib. (10^{-6})	Set B	Set C	Set D
R(T)	16000 cps	0.02	.045		0.2	
$R_o(T)$	40000 cps	0.02	.052		0.2	
τ	3 μsec	1.0	.75	10.0		
u	0.07 cm^2/g	0.1	1.00			0.4
$\ell(T_1)$	2.0 cm	0.05	.25			
T_1	300 K	1.0	.0004			
T	700 K	1.0	.002			
α	7×10^{-6}/K	10.0	.079			
$\rho(T)$	7.127 g/cm^3	±0.15%		±0.87%	±0.34%	±0.41%*

*Same results using $\ell(T_1)$ ± 0.4%.

each of which contributes to the variance as indicated in the table. The summation of the vertical column of variance contributions is identically the summation in Eq. (23), and yields the standard deviation of the resultant $\rho(T)$. Sets B, C, and D are included to show the effect on the resultant $\rho(T)$ precision due to changes in some of the parameters from the base case defined by Set A.

The second method described for calculating the density is Eq. (8). While not including the analytical expression for $\sigma(\rho)$ which corresponds to Eq. (23), it should be noted that the sensitivity to R, R_o, τ, α, and T will be similar, and that $\sigma(\rho_1)/\rho_1$ (at T_1) will contribute directly to $\sigma(\rho_2)/\rho_2$ (at T_2), as do u and ℓ_1 in Eq. (23). To employ Eq. (8), an independently-measured value of ρ in the melt is needed. Crawley [14] has reviewed several methods for liquid metal density measurements; it appears that 0.2% may be a typical error for other methods. Using the above numerical example and $\rho(300\ K) = 7.30\ g/cm^3 \pm 0.2\%$ in Eq. (8) gives $\rho(700\ K) = 7.018\ g/cm^3 \pm 0.21\%$. The same result obtains for an uncertainty in τ of $\pm$ 10%; indeed, this method is extremely insensitive to the imprecision of τ. It is, as expected, very sensitive to the uncertainty in $\rho(T_1)$. The accuracy of a value for $\rho(T_1)$ is the limiting factor in the resultant error of $\rho(T_2)$. Table II summarizes these results.

The third calculational method for determining ρ at a temperature T_2 was given by Eq. (10). Again, the fractional standard deviation $\sigma(\rho_2)/\rho_2$ was calculated from the contributions to the variance $\sigma^2(X_i)$ from each parameter. Inserting the standard set of values leads to $\rho(700\ K)$ with an uncertainty 0.23%. The relation

$$f = 1 + (10^{-5})(T_2 - T_1) \qquad (24)$$

TABLE II

Method 2. $\rho(T_2)$ calculated from Eq. (8). See Table I caption for additional notes.

Parameter		Set A		%Standard Deviation		
		% Standard Deviation	Variance Contrib. (10^{-6})	Set B	Set C	Set D
$\rho(T_1)$	7.30 g/cm^3	0.2	4.0	0.5		
$R(T_1)$	15400 cps	0.02	.041			0.2
$R_o(T_1)$	40000 cps	0.02	.048			0.2
$R(T_2)$	16000 cps	0.02	.044			0.2
$R_o(T_2)$	40100 cps	0.02	.052			0.2
τ	3 μsec	1.0	.0002		10.0	
T_1	300 K	1.0	.00002			
T_2	700 K	1.0	.0001			
α	7 x 10^{-6}/K	10.0	.078			
$\rho(T_2)$	7.018 g/cm^3	±0.21%		±0.50%	±0.21%	±0.48%

was used in Eq. (10) for this calculation, so that $I_o(T)$ increases 0.1% per 100 K. The primary contributions to the uncertainty in $\rho(T_2)$ using Eq. (10) are from $\rho(T_1)$ (± 0.2%) and f (± 0.1%). (This uncertainty in f allows that the value 10^{-5} in Eq. (24) may be in error as much as 25%.) As expected, the sensitivity to τ is small; in fact, an error in τ of as much as 50% had little effect on $\rho(T_2)$. It was found that $\rho(T_2)$, using Eq. (10), is particularly insensitive to u and ℓ_1. This is because u and ℓ_1 enter into the second term in Eq. (10), which is basically the correction added to $\rho(T_1)$ due to the change in temperature to T_2. For the above result, errors in ℓ_1 and u of 2% had little effect on the result. Table III summarizes these findings.

In each of the three methods described, resultant error due to uncertainties in T and α was very small. Similarly, the values of count rate intensities ± 0.02% were sufficiently precise to cause negligible error in the calculated density. Increasing the rate uncertainties to 0.2%, which represents a 100X reduction in counting time, approximately doubles the resultant uncertainty in the density, for the examples given.

In calculating the mean volumetric expansion (using Eq. (11)) and its uncertainty, R_o and R were chosen as above (± 0.02%), with values such that $\alpha_\rho \sim 10^{-4}$/K. Values for τ and α were unchanged. Using a precision for T of ± 0.2%, the resultant uncertainty in α_ρ was ±2.3%, ± 4.5%, and ± 8.6% for $\Delta T = (T_2 - T_1)$ of 200 K, 100 K, and 50 K, respectively. Constant systematic errors in absolute temperature are insignificant, since only temperature differences are important.

To summarize, methods 2 and 3 (Eq. (8) and (10)) are relative density methods, and therefore only yield values for ρ as good as the input value $\rho(T_1)$. The subsequent error introduced by the remaining parameters has been shown to be small, however, so that the technique offers good precision for volumetric

TABLE III

Method 3. $\rho(T_2)$ calculated from Eq. (10). See Table I caption for additional notes.

Parameter		Set A		% Standard Deviation		
		% Standard Deviation	Variance Contrib. (10^{-6})	Set B	Set C	Set D
$\rho(T_1)$	7.30 g/cm^3	0.2	4.3		0.5	
$R(T_1)$	15400 cps	0.02	.045			
$R(T_2)$	16000 cps	0.02	.045			
τ	3 μsec	1.0	.0004	50.0		
u	0.07 cm^2/g	0.1	.001	2.0		
$\ell(T_1)$	2.0 cm	0.05	.0003	2.0		
f	1.004	0.1	1.0			0.4
T_1	300 K	1.0	.0004			
T_2	700 K	1.0	.002			
α	7 x 10^{-6}/K	10.0	.078			
$\rho(T_2)$	7.022 g/cm^3	±0.23%		±0.28%	±0.53%	±0.46%

thermal expansion coefficients. To measure the absolute density ρ in the melt, Method 1 (Eq. (7)) is used. As a practical matter, uncertainties in measurement of I_o, already discussed, can lead to an error in ρ of as much as a few percent with this method.

V. RESULTS AND DISCUSSION

In this section, data are presented for density and thermal expansion measurements using the gamma attenuation technique on several liquids, a solid, and a glass in the transition region. These results are representative of the types of measurements that can be achieved with the technique and agree very favorably with published data, where it exists.

A. Density of Molten Metals

To experimentally verify the utility and precision of the gamma attenuation technique, the liquid metals tin, lead, and aluminum were chosen for study. These materials were selected for two reasons. First, extensive data are available from the literature for these metals, allowing comparison of the results from this work with measurements from higher-precision techniques. Second, since the sensitivity of measurement of the gamma technique depends on the sample density, materials covering a range of densities were investigated ($\rho(Al) \sim 2.4$ g/cm^3, $\rho(Sn) \sim 7.0$, $\rho(Pb) \sim 11.0$).

These measurements were all made using the 1300 K apparatus shown in Fig. 1. The sample materials were fabricated from polycrystalline rods, with purity 99.999$^+$%. Graphite crucibles (POCO AXM-5Q) were used throughout, and the atmosphere was vacuum or Ar at 4 psig. The data were analyzed using Method 3 (above), which requires a value for the density ρ at some temperature in the melt. The data given in the review by Crawley [14] were used for density values at temperatures just above the melting point. (The Crawley paper is a good review of available liquid density measurements.)

1. Tin. The density data for tin (mp 505 K) are shown in Fig. 4. The data points in the figure are the results of several different runs. Curve 1 is a linear fit for $\rho(T)$ recommended by Crawley [14]; this fit is based on the

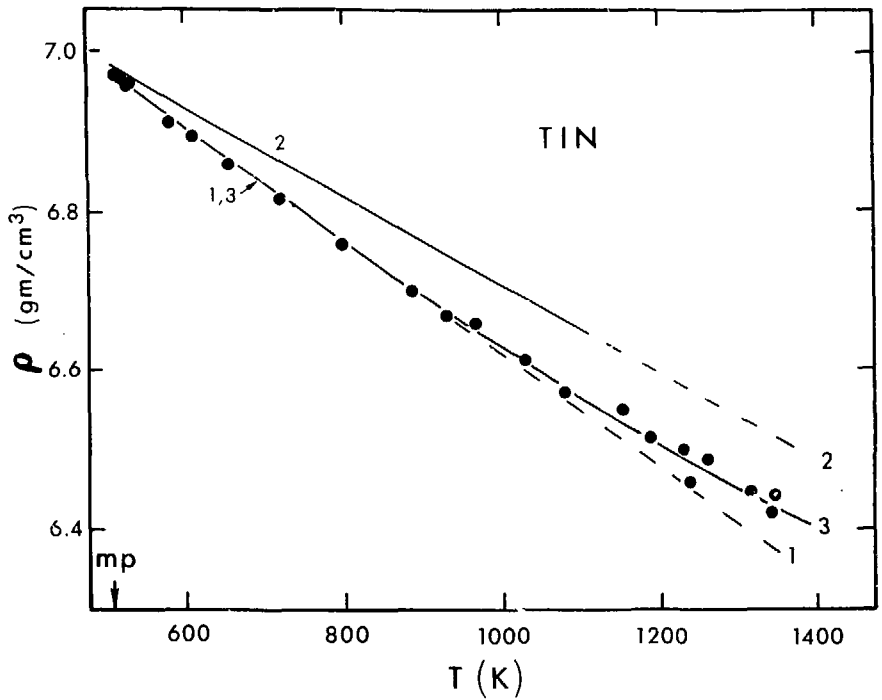

Figure 4. Density vs temperature for molten tin. Curve 1 is the fit recommended by Crawley [14] to 800 K. Curve 2 shows the fit by Berthou and Tougas [16]. Curve 3 is a quadratic fit to the data points, this work.

pycnometric measurements of Thresh, et al. [15], and applies only over a temperature range 505 K to 800 K. In this range, the agreement between the data points and the recommended fit is excellent. The recommended fit is shown extended to higher temperatures in order to display the departure from linearity. Curve 2 is the linear fit from the work of Berthou and Tougas [16], using the Archimedean method to 1100 K. This is included in order to show the differences which exist in the literature. These differences are beyond the experimental error quoted by each investigator (typically less than 0.2%), indicating probable systematic errors between the measurement techniques. Table IV summarizes these and other recent measurements on Sn, by various methods, and shows the spread in the data. Each data set has been fit to an equation of the form

$$\rho(T) = a + b(T - T_m) + c(T - T_m)^2 \qquad (25)$$

where ρ is in g/cm^3, T and T_m are in K, and T_m is the melting temperature. Both linear and quadratic fits to the data points of this work are included for comparison with other investigations. Most investigators use only a linear fit ($c = 0$) due to the limited temperature range measured. Curve 3 is a least-squares quadratic fit to the data in this work. The agreement with the quadratic fit to recent measurements by Desré and Lucas [17] is quite good. They used the Archimedean method over a similarly large temperature range (505 K - 1373 K) and also saw a slight curvature in $\rho(T)$. Recall that the results of this work were based on a value for $\rho(T_m)$ from another work. Therefore, the coefficient a is essentially a fixed parameter; the small differences in the coefficient a result from the details of the fit.

2. Lead. Figure 5 shows the density versus temperature for lead (mp 601 K) from this work. The line is the curve recommended by Crawley [14], based on the pycnometric measurements of Thresh, et al. [15], to 800 K, which

TABLE IV

$\rho(T)$ for Tin - Coefficients in $\rho(T) = a + b(T - 505\ K) + c(T - 505\ K)^2$

Reference	Method	Maximum T Reported (K)	$a(g/cm^3)$	$b(10^{-4}\ g/cm^3\ K)$	$c(10^{-7}\ g/cm^3\ K^2)$
Thresh, et al. [15] (1968)	Pycnometric	800	6.974	-7.125	0
Berthou & Tougas [16] (1968)	Archimedean	1100	6.980	-5.5	0
Döge [3] (1966)	Gamma Attenuation	1473	6.991	-6.57	0
this work (1979)	Gamma Attenuation	1340	6.962	-6.50	0
Desré and Lucas [17] (1977)	Archimedean	1373	6.982	-7.559	1.035
this work (1979)	Gamma Attenuation	1340	6.973	-7.69	1.47

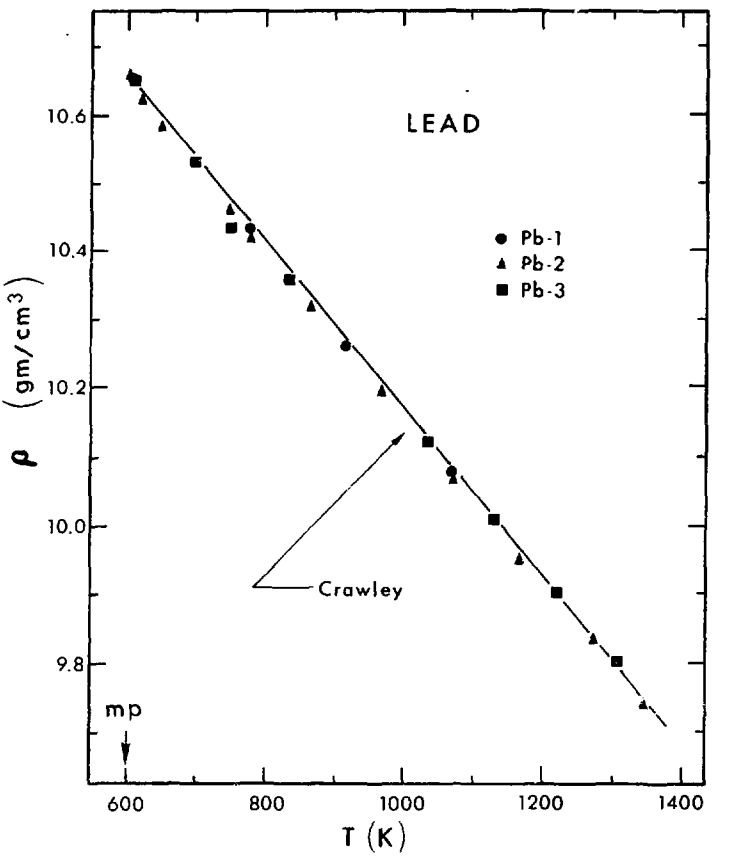

Figure 5. Density vs temperature for molten lead. The line is the fit recommended by Crawley [14].

agrees with our results to 1340 K. Our data are sufficiently fit by a linear equation for $\rho(T)$ over the range 601 K - 1340 K. The data from three separate runs are shown in order to display the reproducibility of the technique. The results are given in Table V, along with results from previous investigations.

3. Aluminum. Figure 6 shows the data for $\rho(T)$ of molten aluminum (mp 933.5 K) from this work, and the linear fits from several other investigators. These fits are given in Table VI. The scatter in our data is due to the low density and therefore low gamma attenuation of Aℓ. However, the slope of our data tends to confirm the results shown in curves 3 and 4, while the expansion coefficient measured by Coy and Mateer [20] appears to be too large. This is significant because the review by Crawley [14] recommends the data of Coy and Mateer depicted by curve 1.

B. Linear Thermal Expansion of Solid Aluminum

Measurements were made on the linear thermal expansion of solid aluminum (polycrystalline, 99.999% purity) using the gamma attenuation technique and the data analysis method described in Section III.B. above. Figure 7 shows the results, plotted as the percentage thermal expansion $\Delta L/L_o$ from a length L_o at ambient temperature (293 K). The data in the figure show the results of two runs, one using a rectangular parallelpiped of Aℓ, and the other a right circular cylinder. For the latter, an effective pathlength through the cylinder was calculated, as discussed in Appendix A. Ambient temperature densities were measured in the laboratory. The curve in Fig. 7 is the recommended thermal expansion of polycrystalline Aℓ given by the Thermophysical Properties Research Center (TPRC) [24]. The agreement with this (primarily dilatometric) data is excellent, particularly in view of the low density, and therefore low attenuation, of Aℓ. This is the first report of

TABLE V

$\rho(T)$ for Lead - Coefficients in $\rho(T) = a + b(T - 601\ K)$

Reference	Method	Maximum T Reported (K)	$a(g/cm^3)$	$b(10^{-4}\ g/cm^3\ K)$
Thresh, et al. [15] (1968)	Pycnometric	800	10.66	-12.22
Schwaneke and Falke [18] (1972)	Maximum Bubble Pressure	820	10.67	-14
Döge [3] (1966)	Gamma Attenuation	1273	10.644	-11.82
Kirschenbaum & Cahill [19] (1961)	Archimedean	1970	10.678	-13.17
Basin & Solov'ev [4] (1967)	Gamma Attenuation	1400	10.674	-12.81
this work (1979)	Gamma Attenuation	1340	10.642	-12.17

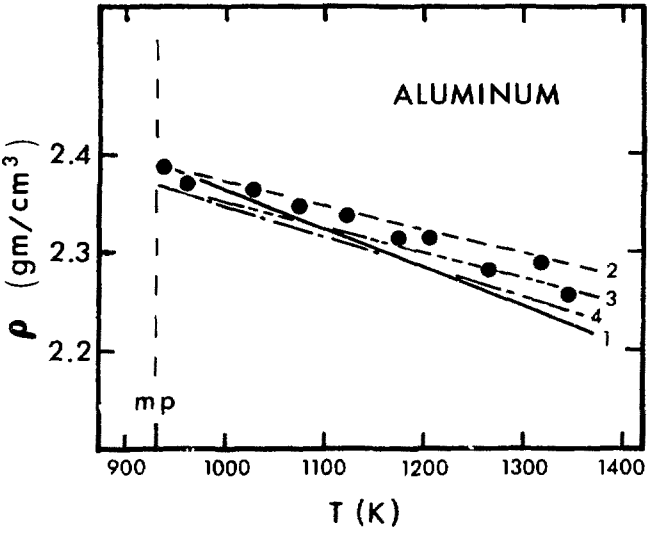

Figure 6. Density vs temperature for molten aluminum. The curves are referenced in Table VI, and represent other investigations using different techniques.

TABLE VI

$\rho(T)$ for Aluminum - Coefficients in $\rho(T) = a + b(T - 933.5\ K)$

Reference	Curve in Fig 6	Method	Maximum T Reported (K)	$a(g/cm^3)$	$b(10^{-4}\ g/cm^3\ K)$
Coy & Mateer [20] (1964)	1	Maximum Bubble Pressure	1180	2.390	-3.954
Naidich & Yeremenko [21] (1961)	2	Pycnometric	1200	2.39	-2.41
Gebhardt, et al. [22] (1955)	3	Archimedean	1170	2.368	-2.60
Gol'tsova [23] (1965)	4	Volumetric	1770	2.369	-3.11
this work (1979)	●	Gamma Attenuation	1340	2.388	-2.92

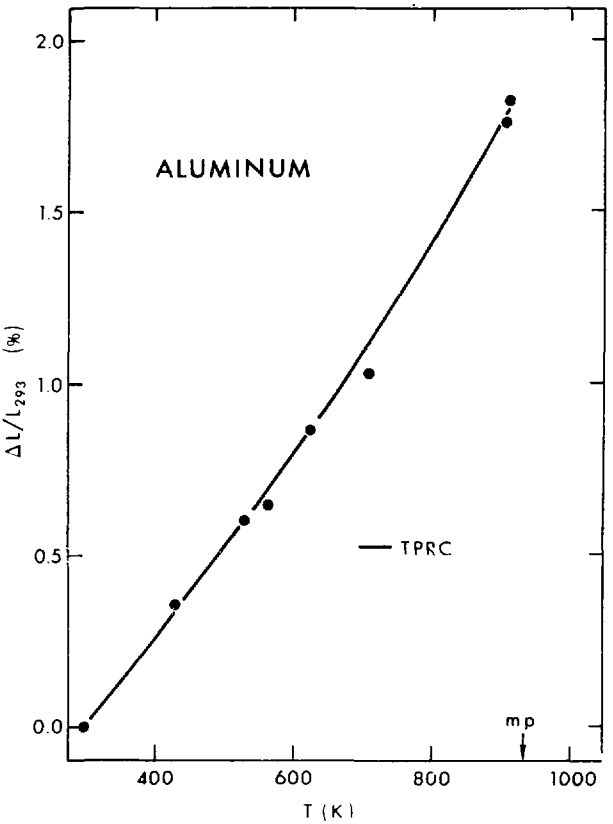

Figure 7. Linear thermal expansion vs temperature for solid aluminum. The line is the expansion recommended by TPRC.

the use of this method for solid thermal expansion measurements. The technique shows promise for use on a variety of materials, especially since the furnace and sample are the only limitations to the temperature range.

C. Thermal Expansion of HD-11 Glass

The density and thermal expansion of a low melting point glass were measured using the gamma attenuation technique. The application of the technique to this type of measurement is unique in that both solid and liquid phase densities may be measured without a change in sample arrangement or measurement technique. The ability to make measurements independent of sample viscosity is particularly useful for the study of glasses through the transition region, where more conventional techniques may not be applied. The material studied was HD-11, primarily a lead silicate glass, supplied by C. J. Leedecke, Sandia Laboratories. This material was chosen for this demonstration study because of its high density (6.13 g/cm^3 ambient) and low glass transition temperature (T_g ~ 420°C).

Fig. 8 shows the linear thermal expansion $\Delta L/L_o$ as measured by the gamma attenuation technique. The lines are visual aids to the reader and indicate the increase in slope at T_g, typical of these materials. This slope discontinuity has often been observed dilatometrically. At temperatures above those shown in Fig. 8, flow occurs, in the region described by "dilatometric softening." This is shown in Fig. 9, where the density length product $\rho\ell$ is plotted vs temperature. The parameter $\rho\ell$ is directly measured using the gamma technique, as in Eq. (1). The product $\rho\ell$ decreases with temperature to about 500°C, then drastically increases, only to decrease with temperature again. This is consistent with thermal expansion of the sample, followed by sample flow near 500°C to conform to the crucible dimension. The occurrence of flow at this temperature is consistent with the

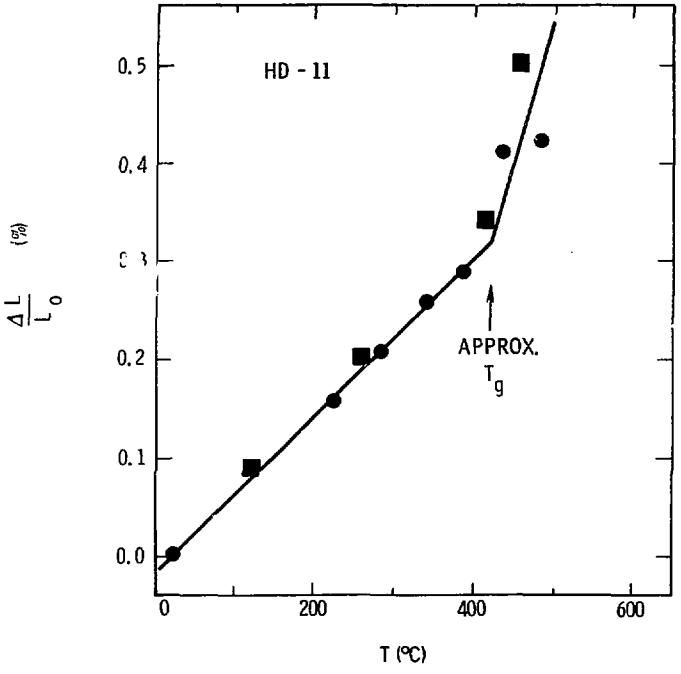

Figure 8. Linear thermal expansion vs temperature for solid HD-11 glass, showing the increase in slope at T_g.

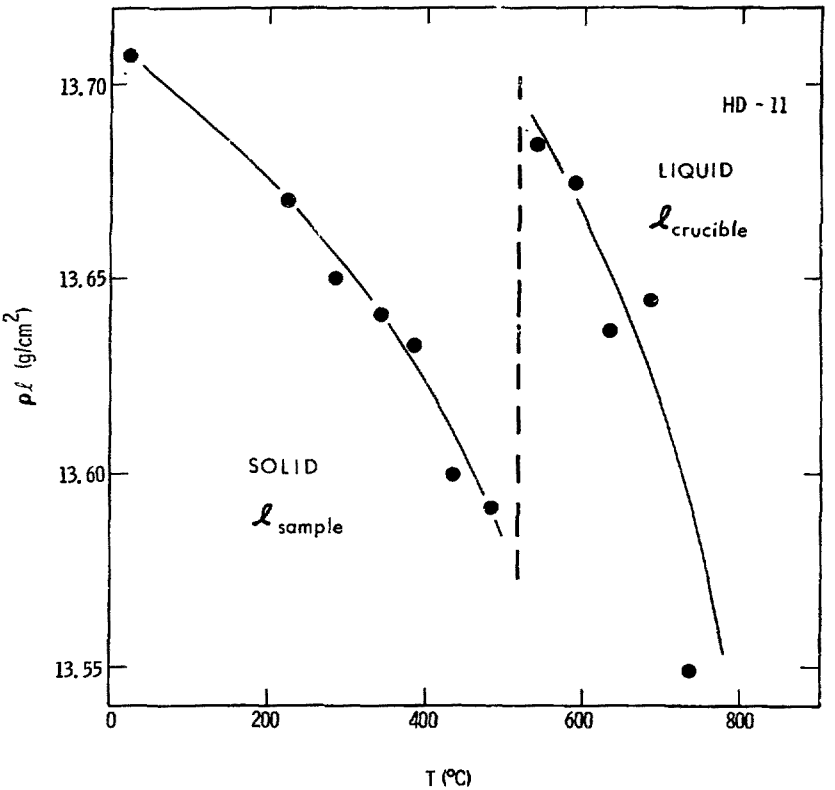

Figure 9. Density length product ρℓ vs temperature for HD-11 glass from ambient to 700°C. This temperature range covers a wide variation in viscosity. The sample is solid at ambient, molten at 700°C, and flows near 500°C conforming to the crucible shape.

viscosity-temperature dependence measured by Rita [25] for a similar composition glass. Using $\ell(T)$ of the sample below 500°C and $\ell(T)$ of the crucible above 500°C yields the plot of ρ versus T shown in Fig. 10 over the temperature range covering both solid and liquid. Note that this analysis removes the discontinuity in $\alpha\ell$ near 500°C, and results in a smooth ρ vs T curve above T_g. The dashed line in Fig. 10 is the volumetric thermal expansion in the melt above 700°C measured by Rita [25] for a similar glass using the Archimedean method. While these results are not intended to represent a definitive study of HD-11 glass, they are at least representative of the type of data which can be obtained by the gamma method on samples with widely-varying viscosities.

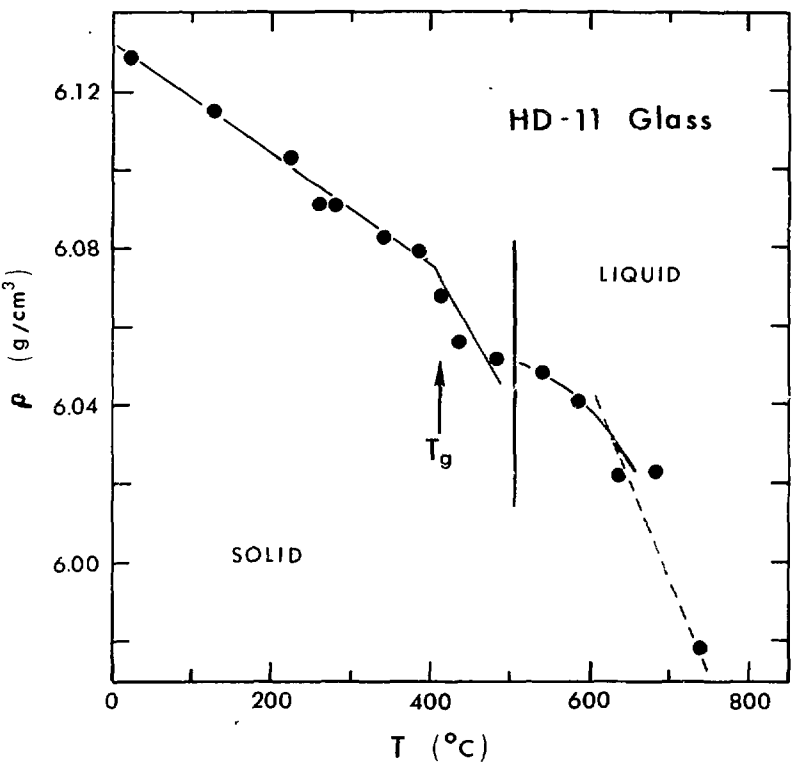

Figure 10. Density vs temperature for HD-11 glass, calculated from the data in Fig. 9. Below 500°C, the sample length (temperature-corrected) was used; above 500°C, the crucible length (temperature-corrected) was used. The dashed curve above 600°C shows the volumetric thermal expansion, measured by Rita [25].

VI. SUMMARY

An apparatus for the measurement of liquid densities at high temperatures using the gamma attenuation method was described, along with an electronic detection system with long-term stability against drift and fluctuations. Using two separate furnace facilities, thermal expansion measurements may be obtained over the range ambient to 3200 K. It has been shown that the following types of data may be obtained using the gamma method:

1. Absolute density measurements vs temperature on molten materials.
2. Volumetric thermal expansion measurements (relative density) on molten materials.
3. Linear thermal expansion measurements of solid materials.
4. Density measurements vs temperature on highly viscous materials, such as glasses.

A particular advantage to this technique is the non-contacting measurement probe. This allows use at very high temperatures and eliminates many of the probe-sample interactions and corrections which accompany other liquid density techniques. In addition, the gamma technique may be used for both solid and liquid phases, or mixtures, such as liquid-saturated particulate beds. Because of these features, the technique may be useful as a diagnostic tool in a variety of field test situations, such as reactor safety studies.

Three data analysis methods for determining the liquid density were presented, along with a precision analysis for each. Depending on the experimental conditions, the methods offer the ability to use different sets of input data, which can be advantageous where experimental determination of some of the parameters is irreproducible or imprecise. In each of the data analysis

methods, the necessary corrections for counting system dead time and crucible expansion have been included.

Method 1 allows determination of the liquid density $\rho(T)$ through Eq. (7) and requires an independent determination of the mass attenuation coefficient for the material. Imprecision in measurement of this coefficient, the system dead time τ, and the crucible dimension ℓ_1 are the most significant contributors to the resultant imprecision in $\rho(T)$.

The second method to calculate $\rho(T)$ uses Eq. (8) and requires independent knowledge of $\rho(T_1)$, the liquid density at some fiducial temperature. However, it does not require precise knowledge of the crucible dimension. Using this method, the resultant imprecision of $\rho(T)$ is primarily due to the error in $\rho(T_1)$ and is relatively insensitive to measurement of the dead time τ.

Method 3 (Eq. (10)) is advantageous for data analysis when specific values for I_o, the gamma intensity through the experimental system in the absence of the sample, are not known. As in Method 2, a value is needed for the liquid density at a single reference temperature; the error in this value is the primary contributor to the resultant imprecision. Uncertainties in the crucible dimension, dead time, and mass attenuation coefficient are relatively unimportant in this data analysis method.

Use of experimentally reasonable values for the input parameters and their precisions yields a similar resultant density precision from the three methods, on the order of 0.2%.

The data analysis was also presented for the use of the gamma attenuation method in the measurement of the linear thermal expansion of solid materials. This is believed to be the first report of the application of this technique to such a measurement.

Representative data were presented for the density vs temperature of molten metals, the linear thermal expansion of a solid, and the density vs temperature for a glass in the transition temperature region. The data agree very well with published results using other methods.

VII. REFERENCES

1. I. G. Dillon, F. E. LeVert, P. A. Loretan, G. U. Menon, F. M. Siddiqi, and H. J. Tarng, Nucl. Tech. 12, 307-313 (1971).
2. F. E. LeVert, I. G. Dillon, and H. J. Tarng, Rev. Sci. Instrum. 44, 313-315 (1973).
3. G. Döge, Z. Naturforschg. 21a, 266-269 (1966).
4. A. S. Basin and A. N. Solov'ev, Zhur. Priklad. Mekh. Tekhn. Fiziki 6, 83-87 (1967).
5. V. I. Yavoyskiy, et al., Russ. Metall. No. 4, 44-47 (1974).
6. W. H. Gardner, G. S. Campbell, and C. Calissendorff, Soil Sci. Soc. Amer. Proc. 36, 393-398 (1972).
7. K. Preiss, Soil Sci. 110, 151-156 (1970).
8. E. Elias, Y. Segal and A. Notea, Nucl. Tech. 21, 57-66 (1974).
9. R. D. Evans, The Atomic Nucleus, McGraw-Hill, New York, 1955.
10. A. Picot, Rev. Sci. Instrum. 47, 385-386 (1976).
11. R. D. Evans, Radiation Dosimetry, Vol. 1, pp. 93-155, Academic Press, New York, 1968.
12. R. J. Reginato, Soil Sci. Soc. Amer. Proc. 38, 156-157 (1974).
13. Y. S. Touloukian, et al. (edit.), "Thermal Expansion," Thermophysical Properties of Matter, Vol. 12, p. 4a (1977).
14. A. F. Crawley, Inter. Metall. Rev. 19, 32-48 (1974).
15. H. R. Thresh, A. F. Crawley and D. W. G. White, Trans. Met. Soc. AIME 242, 819-822 (1968).
16. P. E. Berthou and R. Tougas, J. Less Common Metals 16, 465-467 (1968).
17. P. J. Desré and L. D. Lucas in Proc. Inter. Symp. on Thermal Expansion, 1977 (to be published).
18. A. E. Schwaneke and W. L. Falke, J. Chem. Eng. Data 17, 291-293 (1972).

19. A. D. Kirshenbaum and J. A. Cahill, J. Inorg. Nucl. Chem. 22, 33 (1961).

20. W. J. Coy and R. S. Mateer, Trans. Amer. Soc. Metals 58, 99 (1965).

21. Y. Naidich and V. Yeremenko, Physics of Metals and Metallography USSR, II, No. 6, 62 (1961).

22. E. Gebhardt, M. Becker and S. Dorner, Aluminium, 31 Nr. 7/8, 315 (1955).

23. E. I. Gol'tsova in L. D. Lucas, "Viscometry and Densitometry, B. Liquid Density Measurements," in Physicochemical Measurements in Metals Research Vol. IV, Part 2 (edit. R. A. Rapp), Interscience, (1970).

24. Y. S. Touloukian, op. cit., p. 2.

25. R. A. Rita, PhD. thesis, University of Illinois at Urbana-Champaign, 1976, (unpublished).

Appendix A. Effective Pathlength Through Cylindrical Samples

An effective pathlength is required for the case where a collimated gamma beam of diameter $2R_\gamma$ passes through a cylindrical sample. In the most general case, the beam traverses along a chord of the cylinder, not a diameter, so that the effective pathlength is shortened by both curvature of the sample cylinder and off-center incidence. The case where any portion of the gamma beam misses the cylindrical sample altogether is excluded from this analysis. The situation is depicted in Fig. A1.

The beam with radius R_γ passes through the shaded portion of the sample cylinder of radius R. The beam center is offset from the diameter of the sample by an amount $\xi = \delta + R_\gamma$. The effective pathlength, $\langle \ell \rangle$, is an average of all pathlengths described by the beam's passage through the sample cylinder. We assume a uniform beam intensity.

The effective pathlength $\langle \ell \rangle$ may be found by calculating the volume common to the sample cylinder and the gamma beam, and dividing by πR_γ^2, since the common volume resembles a right circular cylinder of average length $\langle \ell \rangle$ and radius R_γ.

We assume the cylindrical sample is parallel to the z-axis and the gamma beam parallels the y-axis. Fig. A2(a) shows one-quarter of the cross-section of the sample cylinder, and Fig. A2(b) shows a cross-section of the gamma beam. The common volume V is found by first integrating the length $y = \ell(x)$ between the limits x_1 and x_2, then integrating along the z-axis over the region of the beam. As seen in Fig. A2(b), the integration limits x_1 and x_2 vary with z. One has

$$V = 2 \int_{-R_\gamma}^{R_\gamma} dz \int_{x_1(z)}^{x_2(z)} dx\, \ell(x) \qquad \text{(A1)}$$

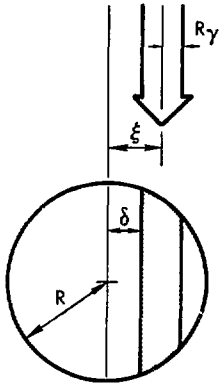

Figure A1. Horizontal cross-section of gamma beam, radius R_γ, passing through a sample cylinder, radius R. The beam may be offset from center by an amount $\xi = \delta + R_\gamma$.

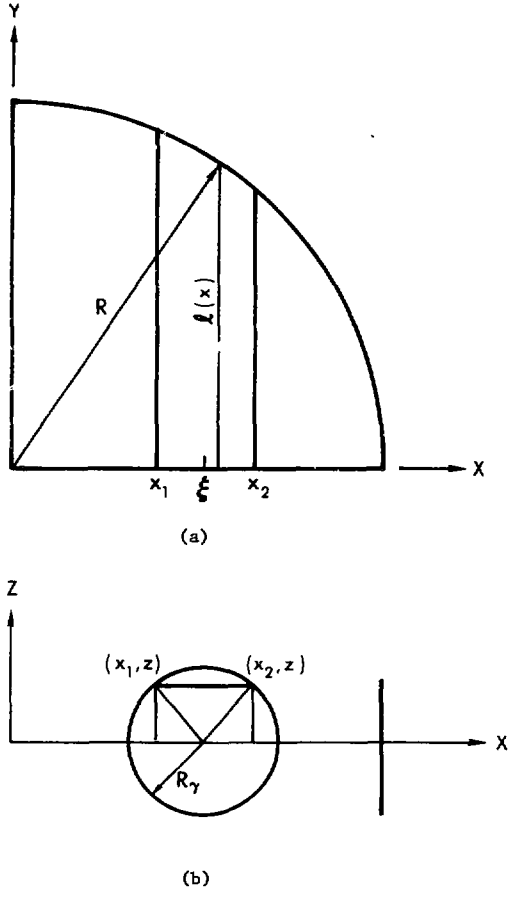

Figure A2. (a) Diagram in XY-plane for integration to determine volume common to the sample cylinder and the (cylindrical) gamma beam. Drawing shows one-quarter of the horizontal cross-section of the sample cylinder.
(b) Diagram in XZ-plane for integration to determine common volume. The integration limits x_1 and x_2 in (a) vary with z as seen in this figure. Drawing is perpendicular to the gamma beam direction, showing the beam cross-section.

where

$$\ell(x) = \left(R^2 - x^2\right)^{\frac{1}{2}} \quad . \tag{A2}$$

Also,

$$x_1(z) = \xi - \left(R_\gamma^2 - z^2\right)^{\frac{1}{2}} \tag{A3}$$

and

$$x_2(z) = \xi + \left(R_\gamma^2 - z^2\right)^{\frac{1}{2}} \quad . \tag{A4}$$

The integral along x is easily done, yielding

$$V = 4 \int_0^{R_\gamma} dz \left\{ \left[\frac{x\left(R^2 - x^2\right)^{\frac{1}{2}}}{2} + \frac{R^2}{2} \sin^{-1}\left(\frac{x}{R}\right) \right] \Bigg|_{x_1(z)}^{x_2(z)} \right\} \quad . \tag{A5}$$

The volume V is readily found from Eq. (A5) using computer methods. Finally,

$$\langle \ell \rangle = V/\pi R_\gamma^2 \quad . \tag{A6}$$

Inserting typical values ($2R_\gamma$ = 0.25 in), one finds $\langle \ell \rangle$ = 1.193 in. for a cylinder of diameter 1.200 in. and no beam offset. To show the effect of the beam offset on $\langle \ell \rangle$, we define the relative error in $\langle \ell \rangle$ to be

$$\frac{\Delta \langle \ell \rangle}{\langle \ell \rangle} = \frac{\langle \ell \rangle - \langle \ell_o \rangle}{\langle \ell \rangle} \quad , \tag{A7}$$

where $\langle \ell_o \rangle$ is the effective length for an offset $\xi = 0$. The relative error in $\langle \ell \rangle$ versus offset ζ is plotted in Fig. A3 for a typical case. Even for an offset of as much as R_γ, the error in $\langle \ell \rangle$ is only about 2%.

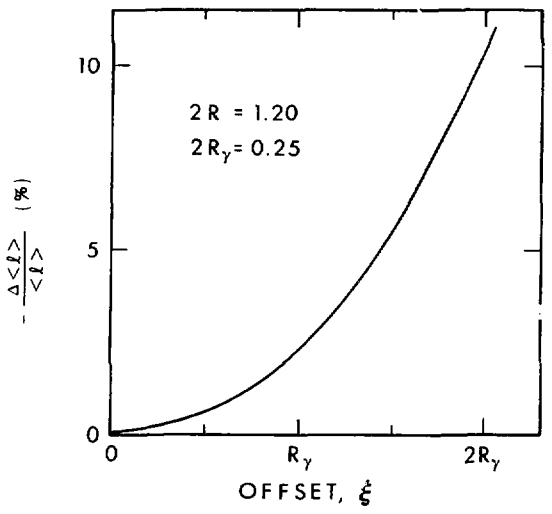

Figure A3. Relative error in effective pathlength due to offset of gamma beam from center of sample cylinder.

Appendix B. Temperature Dependence of I_o Due to Crucible Expansion

Consider a crucible of wall thickness ℓ, density ρ, mass attenuation coefficient u, and linear thermal expansion coefficient α. The temperature-dependent count rate through the crucible is

$$I_o(T) = I_o \exp\ [-u\rho(T)\ell(T)] \quad . \tag{B1}$$

Defining ρ_1 and ℓ_1 at T_1, etc., one has

$$\frac{I_o(T_2)}{I_o(T_1)} = \exp\ [-u(\rho_2\ell_2 - \rho_1\ell_1)] \quad . \tag{B2}$$

For most crucible materials, $(u\rho\ell)$ is typically 0.1 to 0.2, so that the exponential in Eq. (B2) may be approximated as

$$\frac{I_o(T_2)}{I_o(T_1)} \cong 1 - u(\rho_2\ell_2 - \rho_1\ell_1) \quad . \tag{B3}$$

We wish to relate the crucible material parameters to ε, the empirically-determined coefficient which describes the linear temperature dependence of I_o by

$$\frac{I_o(T_2)}{I_o(T_1)} = 1 + \varepsilon(T_2 - T_1) \quad . \tag{B4}$$

Combining Eq. (B3) and (B4) yields

$$\varepsilon = \frac{-u}{\Delta T}(\rho_2\ell_2 - \rho_1\ell_1) \quad , \tag{B5}$$

where $\Delta T = T_2 - T_1$. Using

$$\ell_2 = \ell_1(1 + \alpha\Delta T) \tag{B6}$$

and

$$\rho_2 = \rho_1(1 - 3\alpha\Delta T) \tag{B7}$$

for isotropic materials, one has

$$\varepsilon = \frac{-u\rho_1 \ell_1}{\Delta T} [(1 - 3\alpha\Delta T)(1 + \alpha\Delta T) - 1] \quad . \tag{B8}$$

Ignoring terms of order $(\alpha\Delta T)^2$, Eq. (B8) simplifies to

$$\varepsilon = 2\alpha u \rho_1 \ell_1 \quad . \tag{B9}$$

For an MgO crucible, Eq. (B9) yields $\varepsilon \sim 3.9 \times 10^{-6}$/K, while experimentally the coefficient was determined to be $\varepsilon \sim 4 \times 10^{-6}$/K, as defined by Eq. (B4).